PHYSICAL REVIEW A **106**, 023106 (2022)

# Multichannel dissociative ionization of ethanol in intense ultraviolet laser fields: Energy correlation between photoelectron emission and fragment recoil

Tomoya Ikuta,[1,2] Kouichi Hosaka,[1,3] Hiroshi Akagi,[1] Fumihiko Kannari,[2] and Ryuji Itakura[1,*]

[1]*Kansai Photon Science Institute, National Institutes for Quantum Science and Technology (QST),*
*8-1-7 Umemidai, Kizugawa, Kyoto 619-0215, Japan*
[2]*Department of Electronics and Electronical Engineering, Faculty of Science and Technologies,*
*Keio University, 3-14-1 Hiyoshi, Kohoku-ku, Yokohama 223-8522, Japan*
[3]*Takasaki Advanced Radiation Research Institute, National Institutes for Quantum Science and Technology (QST),*
*1233 Watanuki-machi, Takasaki, Gunma 370-1292, Japan*

(Received 31 December 2021; revised 15 June 2022; accepted 29 July 2022; published 10 August 2022)

We investigate multichannel dissociative ionization of ethanol in intense ultraviolet laser fields using a photoelectron-photoion coincidence momentum imaging technique. Product channels are clearly separated with detected photoions, and channel-specific photoelectron spectra exhibit multiple spectral components unambiguously assigned to four- and five-photon ionization to the electronic ground state and the electronically excited state. We measure kinetic energy distributions of fragment ions as a function of the energy of a correlated photoelectron to reveal how much energy is provided to the fragment recoil of fragment ions in the course of photoelectron emission and subsequent electronic excitation. Subsequent electronic excitation rather than photoelectron emission governs the internal energy of ethanol cations. The role of subsequent electronic excitation becomes more decisive as the laser intensity increases.

DOI: 10.1103/PhysRevA.106.023106

## I. INTRODUCTION

When molecules are exposed to intense laser fields, electrons in molecules are strongly perturbed. Consequently, ionization and electronic excitation take place leading to structural deformation [1–3] and chemical bond breaking [4–6]. Photoelectron emission is an important first step in a variety of reaction processes induced by an intense laser pulse. One of the characteristic features of molecules in intense laser fields is that a number of reaction channels are opened through sequential processes of photoelectron emission and subsequent electronic excitation within a laser pulse. Selective control of multichannel reactions was optimally performed using a laser-pulse shaping technique with a learning algorithm [7–9]. To obtain even higher selectivity of an arbitrary reaction channel, we should thoroughly understand how laser-induced reaction processes proceed. In particular, correlated dynamics of photoelectron emission and electronic excitation is important to understand the entire course of multichannel dissociative ionization in intense laser fields.

It has been understood that a photoelectron is emitted not only from the highest occupied molecular orbital (HOMO), but also from an inner valence orbital even in intense laser fields [10–17]. In other words, ions are prepared not only in the electronic ground state, but also in electronically excited states at the moment of photoelectron emission. Electronic excitation subsequent to photoelectron emission is also possible to proceed within the same laser pulse [10,16–24]. It was also revealed that structural deformation of the parent ion induces nonadiabatic electronic excitation [25,26]. In a series of previous studies monitoring the ion yields in dissociative ionization of ethanol, it was found that the relative yield of $C_2H_5^+$ with respect to $CH_2OH^+$ is enhanced by using stretched laser pulses [9,27,28] and controlled by changing the delay between two laser pulses [29,30]. After $C_2H_5OH^+$ is prepared from the neutral ethanol, it takes a certain time for $C_2H_5OH^+$ to be deformed to the structure where nonadiabatic electronic excitation is significantly enhanced [25]. To understand further details of dissociative ionization dynamics, we will clarify how the electronically excited states are prepared, and how much internal energy gained from a laser field is flown into the dissociation mode. Photoelectron and photoion coincidence momentum imaging (PEPICO-MI) is a powerful method to reveal the correlation between photoelectron emission and fragment recoil [10,31–34].

Using PEPICO-MI with linearly polarized intense near-infrared (NIR) laser fields ($\lambda \sim 783$ nm), we revealed the energy correlation between a photoelectron and a photoion produced from an ethanol molecule $C_2H_5OH$ [22]. Photoelectron emission from the HOMO 3a″ to prepare the electronic ground state of $C_2H_5OH^+$ was clearly identified not only in the channel yielding $C_2H_5OH^+$, but also in the other channels yielding the fragment ions. At the laser intensity of $I_0 = 9\ \mathrm{TW/cm^2}$, the photoelectron spectrum correlated to the $CH_2OH^+$ formation was found to exhibit the broad spectral feature, which was ascribed to photoemission from the inner valence orbital 10a′ (HOMO-1) to prepare the first electronically excited state.

In our previous study [22], the measured energy correlation between a photoelectron and a fragment ion implied

---

[*] itakura.ryuji@qst.go.jp

that the kinetic energy distributions of fragment ions depend on the pathways of photoelectron emission and subsequent electronic excitation. From the kinetic energy distributions of $CH_2OH^+$ as a function of the photoelectron energy, it was suggested that photoelectron emission preparing the electronic ground state of $C_2H_5OH^+$ is correlated to the formation of $CH_2OH^+$ with larger kinetic energy gained in the course of subsequent electronic excitation, and that photoelectron emission preparing the electronically excited state of $C_2H_5OH^+$ is correlated to the formation of $CH_2OH^+$ with smaller kinetic energy. However, when using the NIR laser field, the photoelectron spectrum with a structureless broad feature contains ambiguity in identification of the pathways of photoelectron emission and electronic excitation.

A series of above-threshold ionization (ATI) peaks assigned to the electronically excited state is energetically shifted from those assigned to the electronic ground state, and the spectral width of the peaks assigned to the electronically excited state is as wide as one photon energy (1.58 eV) of the NIR laser fields. As the ionization probability to the electronically excited state becomes comparable to that to the electronic ground state, two series of ATI peaks are smoothly connected, resulting in the structureless broad feature of the photoelectron spectra for the $CH_2OH^+$ formation in the NIR laser fields. Thus, it is difficult to decompose the peaks assigned to different electronic states in the photoelectron spectra when the NIR laser fields are used. If we use a ultraviolet (UV) laser field, whose photon energy is twice as large as that of the NIR fields, the energy spacing between peaks in the ATI spectra becomes sufficiently large for decomposing the peaks in the photoelectron spectra into the different electronic states of $C_2H_5OH^+$ [23].

In the present study, we focus on the kinetic energy distributions of fragment ions produced from $C_2H_5OH^+$ in intense UV laser fields. On the basis of unambiguous identification of the pathways of photoelectron emission and electronic excitation for the formation of the respective fragment ions, we will make sure of the correlation of the dissociative ionization pathways with the kinetic energy distributions of the fragment ions, and then reveal how much internal energy is gained by $C_2H_5OH^+$ in the respective pathways.

## II. EXPERIMENTAL

Details of our experimental apparatus for PEPICO-MI was described in previous publications [10,22,23], and the experimental raw data analyzed in this study are identical to those in Ref. [23]. Briefly, a skimmed effusive beam of pure ethanol vapor is introduced into an ultrahigh vacuum chamber. UV laser pulses are obtained by frequency doubling of output pulses from a regenerative Ti:sapphire amplifier (1 kHz, 796 nm, 38 fs, 2 mJ/pulse) with a $\beta$-BBO crystal (Type I, 0.1 mm thick) and focused on an effusive ethanol beam. The temporal pulse duration of the UV pulse (400 nm) is measured to be 96 fs (full width at half maximum) with a self-diffraction frequency-resolved optical gating technique [35,36]. Dispersion of optical materials such as a lens and a window of the vacuum chamber is taken into account. The laser intensity is adjusted by changing the aperture size of an iris.

Electrostatic lenses installed in the ultrahigh vacuum chamber guide a photoelectron and a product ion on respective position sensitive detectors (RoentDek, HEX80) with a three-dimensional focusing condition [37,38]. The sample gas pressure is kept sufficiently low for ensuring the coincidence detection of an electron and an ion produced from an identical molecule. The detection rate is set to be around 0.3 events per laser shot. The position-sensitive detectors provide a pair of three-dimensional (3D) data, that is, arrival position and time of an electron and an ion, which are recorded shot by shot through time-to-digital converters (RoentDek, TDC8HP).

The provided data are converted into two 3D momenta of an electron and an ion on the basis of the precise trajectory simulation using commercially available software (Scientific Instrument Services, SIMION). In this study, we calibrate momenta of electrons and fragment ions more carefully than in the previous study [23]. The precise structure of the electrostatic lenses, flight tubes, and detectors is included in the trajectory simulation. Nevertheless, the scale of the electron momentum along the detector surface is not matched to that along the time-of-flight axis. The electron momentum converted from the detector surface position is further multiplied by 1.06 to be the same scale as the momentum along the time-of-flight axis. The electron momentum along the time-of-flight axis is simply proportional to the static electric field at the laser-molecule interaction point and thus less influenced by the electric field distortion in the electrostatic lenses. Using the scaled momentum, the energy spacing between the peaks for the four- and five-photon ionization to the electronic ground state in the photoelectron spectra for the formation of $C_2H_5OH^+$ becomes 2.95 eV, which is slightly smaller than one-photon energy 3.10 eV of 400-nm pulses. Although this discrepancy might result from the insufficient correction of the systematic errors in the measurement, there might be another possibility such as the volume effect at the focal area and the influence by intermediate Rydberg states. Thus, we do not make the additional modification of the momentum scale and regard this discrepancy as the uncertainty in the present experiment. Regarding the ion momentum, the converted momentum based on the trajectory simulation is used without any multiplication.

The laser intensity is estimated from the ponderomotive energy shift of the peak of the four-photon ionization correlated with the $C_2H_5OH^+$ formation. In our previous study [22], we estimated the laser intensity from the recoil momenta of $D_2^+$ ionized from $D_2$ by a circularly polarized laser field [39]. The intensities estimated by the two different ways were in good agreement within 30%, which is regarded as the uncertainty in the measurement. The intensity values are updated from those in the previous report [23], but the difference is within the uncertainty.

## III. RESULTS AND DISCUSSION

### A. Channel-specific photoelectron spectra

Kinetic energy of a detected photoelectron is obtained from its measured 3D momentum vector. It is not necessary to perform any numerical processes such as an inverse Abel transformation of a projected image. Channel-specific

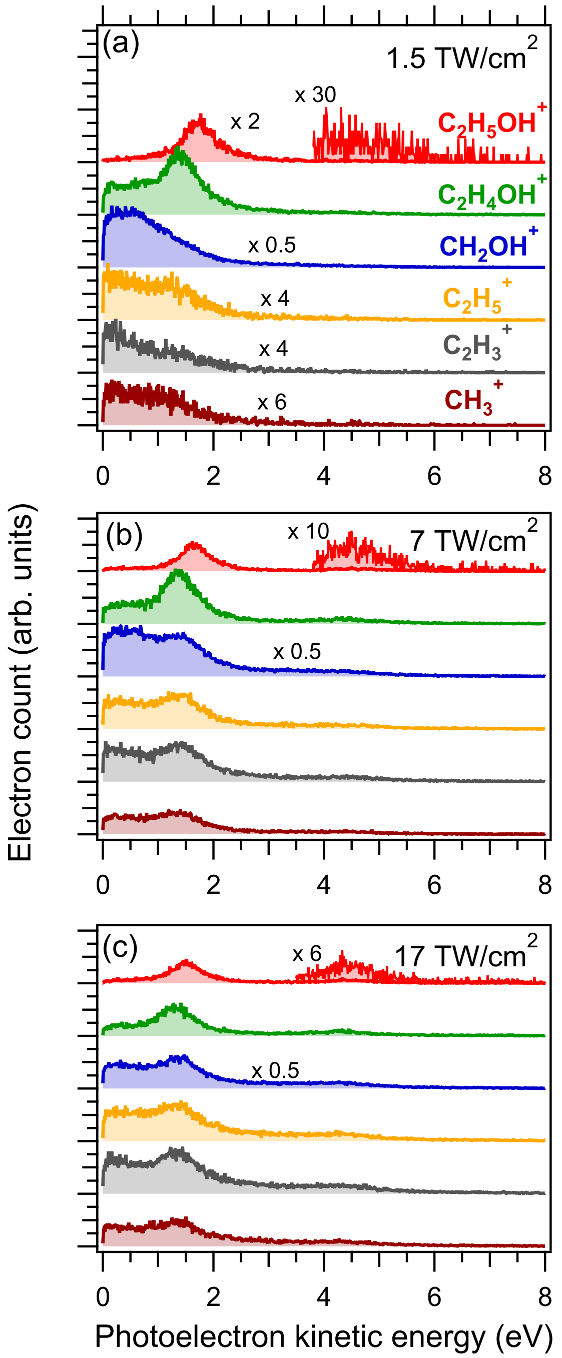

FIG. 1. Channel-specific photoelectron spectra for the formation of $C_2H_5OH^+$ (red), $C_2H_4OH^+$ (green), $CH_2OH^+$ (blue), $C_2H_5^+$ (yellow), $C_2H_3^+$ (gray), and $CH_3^+$ (brown) from the top at the laser peak intensities $I_0$ of (a) 1.5, (b) 7, and (c) 17 TW/cm$^2$. Some of spectra are multiplied as written in figures for ease of viewing. For the $C_2H_5OH^+$ formation, the spectra in the high-energy region assigned to five-photon ATI are vertically expanded.

photoelectron spectra for the formation of $C_2H_5OH^+$, $C_2H_4OH^+$, $CH_2OH^+$, $C_2H_5^+$, $C_2H_3^+$, and $CH_3^+$ are shown in Figs. 1(a)–(c) at the laser peak intensities of $I_0 = 1.5$, 7, and 17 TW/cm$^2$, respectively. The photoelectron energy indicates the intermediate state of $C_2H_5OH^+$ at the moment of photoelectron emission. Subsequent to photoelectron emission, electronic excitation and fragmentation might occur.

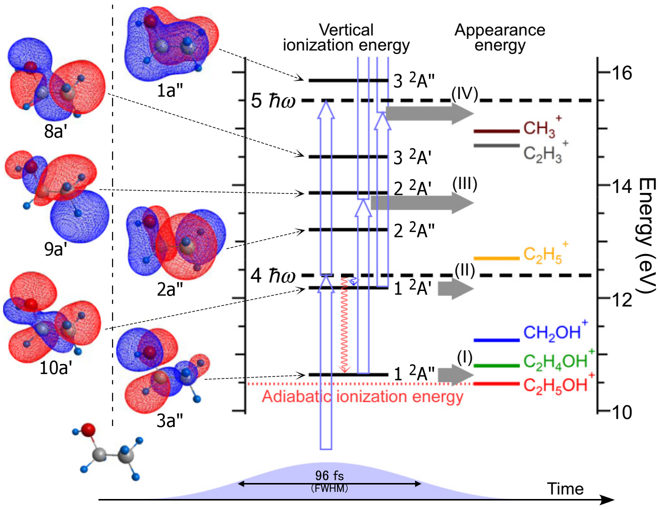

FIG. 2. Schematic energy-level diagram of electronic states of $C_2H_5OH^+$ [40] and appearance energies for $C_2H_4OH^+$, $CH_2OH^+$, $C_2H_5^+$, $C_2H_3^+$, and $CH_3^+$ [41–43]. The energy levels of the electronic ground state $1^2A''$ and the electronically excited states $1^2A'$, $2^2A''$, $2^2A'$, $3^2A'$, and $3^2A''$ are also depicted. The adiabatic ionization energy is shown by a dotted line (red). The energies of four and five photons are shown by dashed lines. The energy is measured from the ground state of neutral ethanol $C_2H_5OH$. Upward arrows indicate one-photon excitation. Right arrows with the labels I–IV indicate reaction paths in terms of excitation energy. On the left side, molecular orbitals from which a photoelectron is ejected to form the respective electronic states are illustrated. These are calculated using density functional theory [B3LYP with the TZV(d,p) basis set].

Measured peaks in the channel-specific photoelectron spectra can be assigned to the electronic ground state and the first electronically excited state unambiguously. The detail of the peak decomposition of the photoelectron spectra was already reported in our previous communication [23]. The features of the photoelectron spectra are briefly described as follows.

In the photoelectron spectra for the $C_2H_5OH^+$ formation in the whole intensity range of $I_0 = 1.5$–17 TW/cm$^2$, a distinct peak is identified in the photoelectron energy region of $E_{\mathrm{elec}} = 1.5$–1.8 eV. This peak is assigned to the four-photon ionization to the electronic ground state $1^2A''$ of $C_2H_5OH^+$ (path I in Fig. 2). Another small peak is also recognized at 3 eV above the distinct main peak and assigned to the five-photon ATI to the electronic ground state. The probability of the five-photon ATI with respect to that of the four-photon ionization increases as the laser intensity increases to 17 TW/cm$^2$.

In the $C_2H_4OH^+$ channel where a hydrogen atom is eliminated, the photoelectron spectra exhibit two components. One is a prominent peak at 0.3 eV below the peak energy in the spectrum of the $C_2H_5OH^+$ channel and assigned to the four-photon ionization to the vibrationally excited states of the electronic ground state (path I in Fig. 2), which is above the threshold energy level for hydrogen elimination [43]. The other is a pedestal in the lower energy side of the main peak and assigned to the four-photon ionization to the first electronically excited state $1^2A'$ (path II in Fig. 2).

In the other fragment channels for the formation of $CH_2OH^+$, $C_2H_5^+$, $C_2H_3^+$, and $CH_3^+$, the four-photon ionization to the first electronically excited state is identified in the

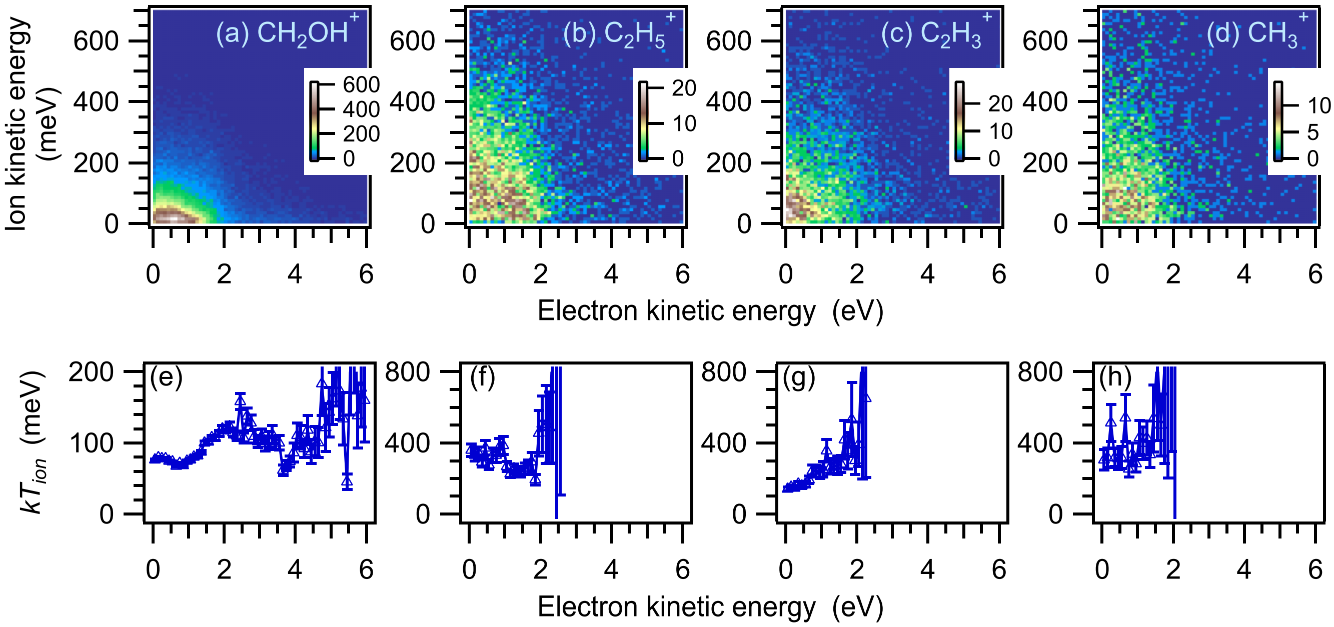

FIG. 3. (a–d) Correlation maps between kinetic energies of a fragment ion and a photoelectron at $I_0 = 1.5$ TW/cm$^2$ for the formation of (a) $CH_2OH^+$, (b) $C_2H_5^+$, (c) $C_2H_3^+$, and (d) $CH_3^+$. (e–h) Temperature $kT_{\mathrm{ion}}$ obtained as a function of the photoelectron energy through fitting of the Boltzmann distribution to kinetic energy distributions of the fragment ions shown in (a)–(d), respectively. Fitting results of the $C_2H_5^+$, $C_2H_3^+$, and $CH_3^+$ channels in the region of $E_{\mathrm{elec}} > 2.5$ eV are not obtained because of insufficient event numbers.

broad energy range of $E_0 < 1.0$ eV in the channel-specific photoelectron spectra, and the four-photon ionization to the vibrationally excited states of the electronic ground state is identified around $E_0 = 1.4$ eV, while the ratio between the ionization probabilities to the two electronic states are different from that in the $C_2H_4OH^+$ channel. The five-photon ATI is also identified in the range of $E_0 = 3$–$5.5$ eV as minor components.

Ethanol cations $C_2H_5OH^+$ survive without fragmentation when they are populated in the lower-lying vibrational states of the electronic ground state through path I shown in Fig. 2. Fragmentation of $C_2H_5OH^+$ proceeds from the vibrationally excited state of the electronic ground state and from the first electronically excited state. The hydrogen elimination and the methyl elimination are opened from the vibrationally excited level of the electronic ground state (path I in Fig. 2) and from the first electronically excited state (path II in Fig. 2), respectively. In the other fragment channels for the formation of hydrocarbon cations, $C_2H_5^+$, $C_2H_3^+$, and $CH_3^+$, subsequent electronic excitation of $C_2H_5OH^+$ (paths III and IV in Fig. 2) occurs necessarily for exceeding the appearance energies of fragmentation [41–43]. The respective peaks in the channel-specific photoelectron spectra can be assigned to the electronic ground state and the first electronically excited state unambiguously [40]. The branching ratios of the respective pathways of photoelectron emission and subsequent electronic excitation were extracted in our previous study [23].

### B. Energy correlation between a fragment ion and a photoelectron

Kinetic energy of fragment ions is a result of all processes of photoelectron emission, subsequent electronic excitation, and fragmentation, while photoelectron energy indicates the energy level of $C_2H_5OH^+$ at the moment of photoelectron emission. As described in Sec. III A, the photoelectron spectral components are securely assigned to the electronic ground state and the first electronically excited state prepared at the moment of photoelectron emission in the respective channels. Here we focus on the correlation between kinetic energies of a fragment ion $E_{\mathrm{ion}}$ and a photoelectron $E_{\mathrm{elec}}$.

Two-dimensional energy correlation maps at $I_0 = 1.5$ TW/cm$^2$ are shown in Figs. 3(a)–(d) for the formation of $CH_2OH^+$, $C_2H_5^+$, $C_2H_3^+$, and $CH_3^+$, respectively. Although the mechanism governing the kinetic energy distribution of fragment ions is unclear, kinetic energy distributions of these fragment ions correlated with a specific $E_{\mathrm{elec}}$ are reproduced well by a functional form of the Boltzmann distribution [22],

$$P_{\mathrm{ion}}(E_{\mathrm{ion}}; E_{\mathrm{elec}}) = A \exp\left(-E_{\mathrm{ion}}/kT_{\mathrm{ion}}\right), \tag{1}$$

where $A$, $k$, and $T_{\mathrm{ion}}$ denote an arbitrary coefficient, the Boltzmann constant, and the temperature as a function of $E_{\mathrm{elec}}$, respectively. The Boltzmann distribution suggests that the intramolecular energy redistribution proceeds in a statistical manner in the course of fragmentation [44]. The temperatures are derived through the least-squares fitting of Eq. (1) to the measured data shown in Figs. 3(a)–(d) and plotted in Figs. 3(e)–(h) for the formation of $CH_2OH^+$, $C_2H_5^+$, $C_2H_3^+$, and $CH_3^+$, respectively. In the fitting process, we take account of the statistical uncertainty in the measured distributions. The standard deviation of the uncertainty is known to be the square root of the detected event number [45]. Considering the large uncertainty, it is not appropriate to discuss the subtle structure appearing in the kinetic energy distributions of the fragment ions. We safely discuss only the degree of the excitation in the fragment recoil using the temperature obtained by fitting of the Boltzmann distribution to the measured distributions.

The temperature $kT_{\mathrm{ion}}$ of the fragment ions reflects how high the excited energy level of $C_2H_5^+OH^+$ is just before fragmentation. In the present experiment with the 400-nm laser pulses, the peaks in the photoelectron energy spectra are securely assigned to the electronic ground state $1^2A''$ and the first electronically excited state $1^2A'$ of $C_2H_5^+OH^+$ as described in Sec. III A. Additionally, the correlation between the fragmentation energy and photoelectron energy allows us to identify the pathways from the electronic states formed at photoelectron emission to the final excited states formed by subsequent photoexcitation in the respective fragmentation channels as discussed below.

In the $CH_2OH^+$ channel, $kT_{\mathrm{ion}}$, decreases from 79 to 68 meV, as the photoelectron energy $E_{\mathrm{elec}}$ increases from 0 to 0.8 eV as shown in Fig. 3(e). The photoelectron energy range of $E_{\mathrm{elec}} = 0$–0.8 eV corresponds to the main peak in the photoelectron spectrum for the $CH_2OH^+$ formation and is assigned to the four-photon ionization to the first electronically excited state, from which the $CH_2OH^+$ formation (appearance energy, 11.25 eV) is energetically possible through path II shown in Fig. 2 [41]. Considering the energy conservation, the measured energy correlation is reasonable. The excess energy is shared by the photoelectron kinetic energy and the internal energy of $C_2H_5OH^+$, part of which is released as the translational energy of the fragments [46].

As $E_{\mathrm{elec}}$ increases from 0.8 to 2.1 eV, $kT_{\mathrm{ion}}$ increases to 120 meV. This increase in $kT_{\mathrm{ion}}$ indicates the transition from path II to path III. Although this photoelectron energy around $E_{\mathrm{elec}} = 2.1$ eV is seemingly covered by the high-energy tail of the main peak in the photoelectron spectrum for the $CH_2OH^+$ formation, it is assigned to the electronic ground state, the peak of which becomes apparent as $I_0$ increases to 7 and 17 TW/cm$^2$, as shown in Figs. 1(b) and 1(c), respectively. When the electronic ground state of $C_2H_5OH^+$ is prepared at the moment of photoelectron emission, subsequent electronic excitation is required for the $CH_2OH^+$ formation through path III. The larger kinetic energy of $CH_2OH^+$ results from the larger excess energy of $C_2H_5OH^+$. Subsequent excitation from the electronic ground state results in larger excess energy than that for the fragmentation from the electronically excited state prepared at photoelectron emission. Therefore, $kT_{\mathrm{ion}}$ in path III is larger than that in path II.

In the photoelectron energy range of $E_{\mathrm{elec}} = 2.1$–5.0 eV assigned to the five-photon ATI, $kT_{\mathrm{ion}}$ is expected to be similar to that in the range of $E_{\mathrm{elec}} = 0$–2.1 eV assigned to the four-photon ionization. Although both ionization processes form the same electronic states of $C_2H_5OH^+$ irrespective of the absorbed photon number in ionization, $kT_{\mathrm{ion}}$ by the five-photon ATI is larger than that by the four-photon ionization. This might be caused by the volume effect at the focal area. It is probable that the five-photon ATI occurs only at the center of the focal spot, while the four-photon ionization occurs in the relatively large volume around the focal spot. As a result, the effective laser intensity for the five-photon ATI might be larger than that for the four-photon ionization. At the larger $I_0$, the number of photons absorbed by $C_2H_5OH^+$ would not be less than two photons in the course of photoexcitation subsequent to photoelectron emission, resulting in the larger $kT_{\mathrm{ion}}$. In the range of $E_{\mathrm{elec}}>5.0$ eV, $kT_{\mathrm{ion}}$ becomes much larger than that in $E_{\mathrm{elec}}<5.0$ eV. The volume effect might be more significant, but quantitative examination is currently difficult because of the large statistical error.

In Fig. 3(f) it is shown that $kT_{\mathrm{ion}}$ of $C_2H_5^+$ decreases from 360 to 193 meV as $E_{\mathrm{elec}}$ increases from 0 to 1.8 eV. This negative correlation between $E_{\mathrm{elec}}$ and $kT_{\mathrm{ion}}$ is interpreted by energy sharing between a photoelectron and a $C_2H_5OH^+$ cation, similarly to that of $CH_2OH^+$ in $E_{\mathrm{elec}} = 0$–0.8 eV. The appearance energy of $C_2H_5^+$ (12,7 eV) lies above the first electronically excited state [41], suggesting that subsequent electronic excitation of $C_2H_5OH^+$ is required for the formation of $C_2H_5^+$ through paths III and IV, irrespective of the electronic states prepared at the moment of photoelectron emission. Thus, the total number of the absorbed photons in the entire course of dissociative ionization is identical for both paths III and IV. As a result, the excess energy of $C_2H_5OH^+$ leading to the $C_2H_5^+$ formation decreases as $E_{\mathrm{elec}}$ increases. In the range of $E_{\mathrm{elec}} > 2.0$ eV, detailed examination is difficult because of the large fitting errors originating from a small number of detected events. Therefore, we do not discuss $kT_{\mathrm{ion}}$ of $C_2H_5^+$ in this $E_{\mathrm{elec}}$ range.

In Fig. 3(g) it is shown that $kT_{\mathrm{ion}}$ of $C_2H_3^+$ linearly increases from 141 to 390 meV as $E_{\mathrm{elec}}$ increases from 0 to 2.0 eV. This positive correlation between $kT_{\mathrm{ion}}$ and $E_{\mathrm{elec}}$ cannot be interpreted by energy sharing between a photoelectron and $C_2H_5OH^+$. For the $C_2H_3^+$ formation, electronic excitation subsequent to photoelectron emission is required because the appearance energy is 14.7 eV, which is even higher than the vertical energy level of the first electronically excited state (12.18 eV) of $C_2H_5OH^+$as shown in Fig. 2 [42]. When the photoelectron energy is nearly $E_{\mathrm{elec}} = 0$ eV in the four-photon ionization, additional one-photon absorption causes the prepared $C_2H_5OH^+$ to be excited to the energy level above the appearance energy. As the photoelectron energy increases to more than $E_{\mathrm{elec}} = 1.0$ eV, two-photon energy is at least required for the $C_2H_3^+$ formation. The increment in the absorbed photon number in subsequent photoexcitation would cause the positive correlation between $kT_{\mathrm{ion}}$ and $E_{\mathrm{elec}}$, similarly to that for the $CH_2OH^+$ formation in the range of $0.8 < E_{\mathrm{elec}}<2.1$ eV [Fig. 3(e)]. Additionally, in the course of the formation of $C_2H_3^+$, three-body dissociation such as $C_2H_3^+ + H + H_2O$ and $C_2H_3^+ + H_2 + OH$ proceeds because $H_3O$ is unstable [47]. Ladder switching excitation [48] so that photoexcitation and structural deformation take place alternately is also probable within the laser pulse duration of 96 fs. The dominant reaction pathway might be changed as a function of $E_{\mathrm{elec}}$. Thus, such complicated reaction dynamics for the $C_2H_3^+$ formation would cause the measured $kT_{\mathrm{ion}}$ profile of $C_2H_3^+$.

For the formation of $CH_3^+$, the appearance energy is 14.95 eV, similar to that for the $C_2H_3^+$ formation [42]. Nevertheless, as shown in Fig. 3(h), $kT_{\mathrm{ion}}$ of $CH_3^+$ as a function of $E_{\mathrm{elec}}$ is different from that of $C_2H_3^+$ and exhibits a nearly constant value of $kT_{\mathrm{ion}} \simeq 400$ meV in the range of $E_{\mathrm{elec}} = 0$–1.5 eV. The difference from that of $C_2H_3^+$ [Fig. 3(g)] would reflect excitation and fragmentation dynamics occurring in the respective exit channels. In the range of $E_{\mathrm{elec}} > 1.5$ eV, the error of $kT_{\mathrm{ion}}$ is too large to discuss in detail.

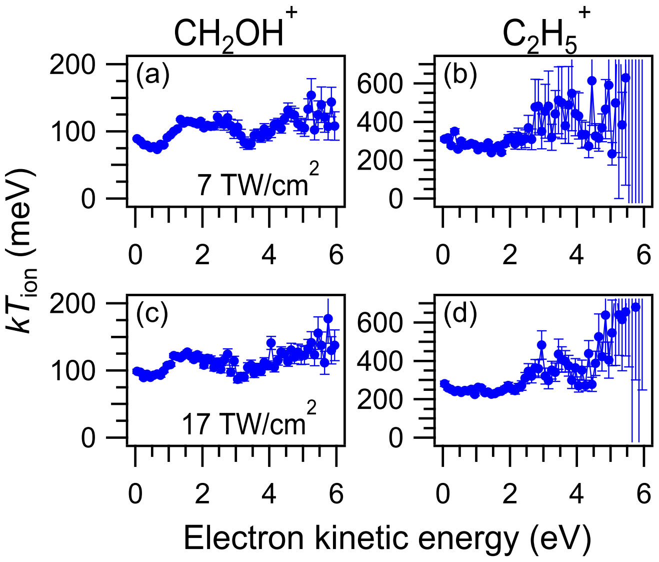

FIG. 4. Temperature $kT_{\text{ion}}$ obtained as a function of the photoelectron energy through fitting of the Boltzmann distribution to kinetic energy distributions of fragment ions at the laser intensities of $I_0 = 7$ (a, b) and 17 TW/cm$^2$ (c, d) for the formation of $CH_2OH^+$ (a, c) and $C_2H_5^+$ (b, d).

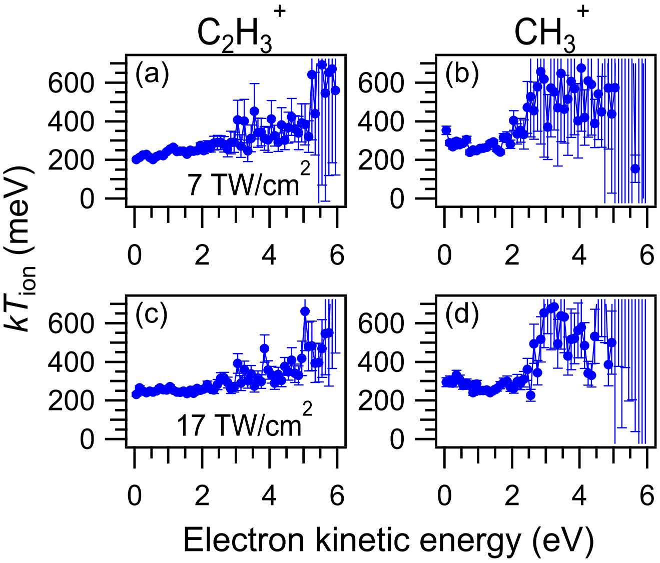

FIG. 5. Temperature $kT_{\text{ion}}$ obtained as a function of the photoelectron energy through fitting of the Boltzmann distribution to kinetic energy distributions of fragment ions at the laser intensities of $I_0 = 7$ (a, b), and 17 TW/cm$^2$ (c, d) for the formation of $C_2H_3^+$ (a, c) and $CH_3^+$ (b, d).

### C. Laser intensity dependence of energy correlation

We examine the laser intensity dependence of energy correlation between a fragment ion and a photoelectron while referring to the channel-specific photoelectron spectra. Figure 4 shows $kT_{\text{ion}}$ of $CH_2OH^+$ and $C_2H_5^+$ derived from the measured energy correlation maps at $I_0 = 7$ and 17 TW/cm$^2$. In the $CH_2OH^+$ channel [Figs. 4(a) and 4(c)], $kT_{\text{ion}}$ as a function of $E_{\text{elec}}$ looks similar to that at $I_0 = 1.5$ TW/cm$^2$, while the shift toward the lower $E_{\text{elec}}$ side by the ponderomotive energy takes place similarly to the photoelectron spectrum. As described in Sec. III A and Ref. [23], the spectral components in the photoelectron spectra shown in Fig. 1 are assigned to the electronic ground state $1^2A''$ and the first electronically excited $1^2A'$ more unambiguously at $I_0 = 7$ and 17 TW/cm$^2$ than at $I_0 = 1.5$ TW/cm$^2$. Therefore, we undoubtedly identify the paths from the electronic states prepared at the moment of photoelectron emission to the final excited energy levels prepared by subsequent photoexcitation leading to the fragmentation into $CH_2OH^+$ and $CH_3$, which are shown as paths II and III in Fig. 2. At $I_0 = 7$ and 17 TW/cm$^2$, $kT_{\text{ion}}$ by the five-photon ATI does not increase significantly from that by the four-photon ionization. This result suggests that difference between the volume effects at the four-photon ionization and the five-photon ATI is reduced in the $CH_2OH^+$ formation as $I_0$ increases from 1.7 to 7 and 17 TW/cm$^2$.

In the $C_2H_5^+$ channel [Figs. 4(b) and 4(d)], the variation of $kT_{\text{ion}}$ in the range of $E_{\text{elec}} = 0$–2.0 eV is suppressed as the laser intensity increases from 1.5 to 7 and 17 TW/cm$^2$. At $I_0 = 17$ TW/cm$^2$, $kT_{\text{ion}}$ as a function of $E_{\text{elec}}$ becomes almost flat around $kT_{\text{ion}} = 250$ meV. Similarly to the $CH_2OH^+$ channel, the spectral components are unambiguously assigned to ionization to the electronic ground state and to the first electronically excited state. The flat $kT_{\text{ion}}$ profile in the $C_2H_5^+$ channel suggests that the electronic and vibrational states prepared at the moment of photoelectron emission do not influence the final excited states leading to the $C_2H_5^+$ formation. As $I_0$ increases, multiphoton excitation of $C_2H_5OH^+$ to higher energy levels than paths III and IV makes a more significant contribution in the entire course of dissociative ionization to form $C_2H_5^+$. If the population in the excited states of $C_2H_5OH^+$ leading to the $C_2H_5^+$ formation is distributed in the wider energy range, the difference in the energy levels at photoelectron emission is less influential. Significant suppression of the $kT_{\text{ion}}$ variation suggests a significant contribution of subsequent multiphoton excitation of $C_2H_5OH^+$ in the $C_2H_5^+$ channel with increasing $I_0$. In the range of $E_{\text{elec}} = 2.5$–4.0 eV assigned to the five-photon ATI, it is found that the $kT_{\text{ion}}$ of $C_2H_5^+$ increases to more than 350 meV. The larger $kT_{\text{ion}}$ would be caused by the volume effect as mentioned above.

In the $C_2H_3^+$ channel [Figs. 5(a) and 5(c)], the $kT_{\text{ion}}$ profile can be approximated by a straight line with a positive slope in the wide energy range of $E_{\text{elec}} = 0$–5.0 eV at $I_0 = 7$ and 17 TW/cm$^2$. The slope decreases as $I_0$ increases from 1.5 to 17 TW/cm$^2$. This feature is also explained by enhancement of subsequent multiphoton excitation of $C_2H_5OH^+$ with increasing $I_0$. Multiphoton excitation subsequent to photoelectron emission plays a more significant role in the $C_2H_3^+$ channel as $I_0$ increases.

In the $CH_3^+$ channel [Figs. 5(b) and 5(d)], the statistical error is significantly suppressed as $I_0$ increases from 1.5 to 7 and 17 TW/cm$^2$. Therefore, we can examine the variation of $kT_{\text{ion}}$ at $I_0 = 7$ and 17 TW/cm$^2$ in more detail than at $I_0 = 1.5$ TW/cm$^2$. The $kT_{\text{Ion}}$ profile is qualitatively similar to that in the $C_2H_5^+$ channel at $I_0 = 7$ and 17 TW/cm$^2$. Therefore, similarly to the $C_2H_5^+$ channel, there is a significant contribution of subsequent multiphoton excitation of $C_2H_5OH^+$ to much higher energy levels than the appearance energy level of 14.95 eV for the $CH_3^+$ formation. As $E_{\text{elec}}$ increases from

$E_{\mathrm{elec}} = 2.5$ eV, $kT_{\mathrm{ion}}$ increases steeply to around 600 meV at $E_{\mathrm{elec}} \simeq 3.3$ eV. This is also interpreted by the volume effect, similarly to $C_2H_5^+$.

The $CH_3^+$ and $C_2H_3^+$ channels have similar appearance energies [42], and their channel-specific photoelectron spectra exhibit the similar spectral feature as shown in Fig. 1. Nevertheless, their $kT_{\mathrm{ion}}$ profiles are quite different, indicating that subsequent electronic excitation and dissociation proceed in different manners in the $C_2H_3^+$ and $CH_3^+$ channels.

It is interesting to compare the kinetic energy distributions of the fragment ions produced by the 400-nm fields with those by the 783-nm fields [22]. When using the 783-nm fields, $kT_{\mathrm{ion}}$ depends on the laser intensity and the pulse duration. As the laser intensity and the pulse duration increase, $kT_{\mathrm{ion}}$ increases monotonically. The intensity and pulse duration were changed from 9 to 23 $\mathrm{TW/cm^2}$ and from 35 to 800 fs, respectively. The measured $kT_{\mathrm{ion}}$ was at the maximum 60 meV (700 K) for $CH_2OH^+$ and 260 meV (3000 K) for $C_2H_5^+$. Meanwhile, when using the 400-nm fields, $kT_{\mathrm{ion}}$ of $CH_2OH^+$ varies in the range of 58–140 meV, and that of $C_2H_5^+$ is around 280 meV. Comparing $kT_{\mathrm{ion}}$ by the 400-nm and 783-nm fields at the similar laser intensity and pulse duration, it is apparent that $kT_{\mathrm{ion}}$ by the 400-nm fields is larger than that by the 783-nm, particularly in the $CH_2OH^+$ channel. It would be ascribed to the difference in one-photon energy. The influence by the one-photon energy difference would be more significant in the $CH_2OH^+$ channel in terms of the ratio of $E_{\mathrm{ion}}$ ($kT_{\mathrm{ion}}$), because the number of absorbed photons to exceed the dissociation threshold is smaller than those in the other channels. Additionally, wavelength dependence on the one-photon and multiphoton excitation probabilities should be important in the internal energy gained from the laser fields. As an alternative theoretical way to describe excitation in intense laser fields, nonadiabatic coupling between time-dependent adiabatic potential energy surfaces can be used [25]. Strength of nonadiabatic coupling between the electronic states in intense laser fields should depend on characteristics of laser fields such as wavelength, pulse duration, and intensity.

## IV. SUMMARY

We have shown that the energy correlation between photoelectron emission and fragment recoil provides abundant information on excitation pathways in multichannel dissociative ionization of ethanol in intense UV laser fields in the laser intensity range of $I_0 = 1.5$–17 $\mathrm{TW/cm^2}$. Using PEPICO-MI, the kinetic energy distributions of the four fragment ions, $CH_2OH^+$, $C_2H_5^+$, $C_2H_3^+$, and $CH_3^+$, have been measured as a function of the energy of the correlated photoelectron. The large photon energy of the 400-nm fields enables us to decompose the peaks in the channel-specific photoelectron spectra into four- and five-photon ionization to the first electronically excited state $1^2A'$ and the electronic ground state $1^2A''$. Consequently, we have unambiguously clarified the electronic states prepared at the moment of photoelectron emission and the resultant kinetic energy distributions of the fragment ions. The contribution of electronic excitation subsequent to photoelectron emission in the respective fragmentation channels has been unveiled. Subsequent electronic excitation plays a more important role in the internal energy gain than photoelectron emission.

In the $CH_2OH^+$ channel, if $C_2H_5OH^+$ is prepared in the electronic ground state at the moment of photoelectron emission, subsequent electronic excitation takes place through path III shown in Fig. 2. Meanwhile, if $C_2H_5OH^+$ is prepared in the first electronically excited state, fragmentation proceeds without subsequent excitation through path II.

In the $C_2H_5^+$, $C_2H_3^+$, and $CH_3^+$ channels, subsequent electronic excitation of $C_2H_5OH^+$ is necessary irrespective of the electronic states prepared at photoelectron emission. Dissociative ionization proceeds through paths III and IV. Additionally, multiphoton excitation causes reaction paths on higher energy levels than path IV. As $I_0$ increases from 1.5 to 17 $\mathrm{TW/cm^2}$, $kT_{\mathrm{ion}}$ is less influenced by the electronic states prepared at the moment of photoelectron emission. Subsequent multiphoton excitation plays an important role in determination of the final internal energy at the higher $I_0$.

In this study, we have demonstrated that PEPICO-MI enables us to trace the reaction pathways in terms of energetics, that is, the electronic states prepared at photoelectron emission and the degree of excitation just before the fragmentation. As a remaining issue, the dynamics in terms of structural deformation is still unclear. Combining PEPICO-MI with time-resolved Coulomb explosion imaging [49] will help us to more clearly visualize how dissociative ionization proceeds.

## ACKNOWLEDGMENTS

We thank Dr. A. Yokoyama and Prof. K. Yamanouchi for their support in the early stage of this work. The present work was financially supported in part by JSPS KAKENHI (Grants No. JP22685004, No. JP26288013, and No. JP17K05089).

---

[1] A. Hishikawa, A. Iwamae, and K. Yamanouchi, Ultrafast Deformation of the Geometrical Structure of $CO_2$ Induced in Intense Laser Fields, Phys. Rev. Lett. **83**, 1127 (1999).

[2] A. Hishikawa, A. Iwamae, and K. Yamanouchi, Ultrafast structural deformation of $NO_2$ in intense laser fields studied by mass-resolved momentum imaging, J. Chem. Phys. **111**, 8871 (1999).

[3] J. H. Sanderson, A. El-Zein, W. A. Bryan, W. R. Newell, A. J. Langley, and P. F. Taday, Geometry modifications and alignment of $H_2O$ in an intense femtosecond laser pulse, Phys. Rev. A **59**, R2567 (1999).

[4] S. L. Chin, Multiphoton ionization of molecules, Phys. Rev. A **4**, 992 (1971).

[5] L. J. Frasinski, K. Codling, P. Hatherly, J. Barr, I. N. Ross, and W. T. Toner, Femtosecond Dynamics of Multielectron Dissociative Ionization by Use of a Picosecond Laser, Phys. Rev. Lett. **58**, 2424 (1987).

[6] C. Cornaggia, J. Lavancier, D. Normand, J. Morellec, P. Agostini, J. P. Chambaret, and A. Antonetti, Multielectron dissociative ionization of diatomic molecules in an intense femtosecond laser field, Phys. Rev. A **44**, 4499 (1991).

[7] A. Assion, T. Baumert, M. Bergt, T. Brixner, B. Kiefer, V. Seyfried, M. Strehle, and G. Gerber, Control of chemical reactions by feedback-optimized phase-shaped femtosecond laser pulses, Science **282**, 919 (1998).

[8] R. J. Levis, G. M. Menkir, and H. Rabitz, Selective bond dissociation and rearrangement with optimally tailored, strong-field laser pulses, Science **292**, 709 (2001).

[9] H. Yazawa, T. Tanabe, T. Okamoto, M. Yamanaka, F. Kannari, R. Itakura, and K. Yamanouchi, Open-loop control and closed-loop control of dissociative ionization of ethanol in intense laser fields, J. Chem. Phys. **124**, 204314 (2006).

[10] K. Hosaka, R. Itakura, K. Yokoyama, K. Yamanouchi, and A. Yokoyama, Photoelectron-photoion coincidence momentum imaging for dissociative ionization of ethanol in intense laser fields, Chem. Phys. Lett. **475**, 19 (2009).

[11] H. Akagi, T. Otobe, A. Staudte, A. Shiner, F. Turner, R. Dorner, D. M. Villeneuve, and P. B. Corkum, Laser tunnel ionization from multiple orbitals in HCl, Science **325**, 1364 (2009).

[12] O. Smirnova, Y. Mairesse, S. Patchkovskii, N. Dudovich, D. Villeneuve, P. Corkum, and M. Y. Ivanov, High harmonic interferometry of multi-electron dynamics in molecules, Nature (London) **460**, 972 (2009).

[13] M. Spanner and S. Patchkovskii, One-electron ionization of multielectron systems in strong nonresonant laser fields, Phys. Rev. A **80**, 063411 (2009).

[14] A. E. Boguslavskiy, J. Mikosch, A. Gijsbertsen, M. Spanner, S. Patchkovskii, N. Gador, M. J. J. Vrakking, and A. Stolow, The multielectron ionization dynamics underlying attosecond strong-field spectroscopies, Science **335**, 1336 (2012).

[15] X. Xie, S. Roither, M. Schöffler, E. Lötstedt, D. Kartashov, L. Zhang, G. G. Paulus, A. Iwasaki, A. Baltuška, K. Yamanouchi, and M. Kitzler, Electronic Predetermination of Ethylene Fragmentation Dynamics, Phys. Rev. X **4**, 021005 (2014).

[16] P. M. Kraus, B. Mignolet, D. Baykusheva, A. Rupenyan, L. Horný, E. F. Penka, G. Grassi, O. I. Tolstikhin, J. Schneider, F. Jensen, L. B. Madsen, A. D. Bandrauk, F. Remacle, and H. J. Wörner, Measurement and laser control of attosecond charge migration in ionized iodoacetylene, Science **350**, 790 (2015).

[17] H. Akagi, T. Otobe, and R. Itakura, Deformation of an inner valence molecular orbital in ethanol by an intense laser field, Sci. Adv. **5**, eaaw1885 (2019).

[18] W. Fuß, W. E. Schmidt, and S. A. Trushin, Time-resolved dissociative intense-laser field ionization for probing dynamics: Femtosecond photochemical ring opening of 1,3-cyclohexadiene, J. Chem. Phys. **112**, 8347 (2000).

[19] R. Itakura, J. Watanabe, A. Hishikawa, and K. Yamanouchi, Ionization and fragmentation dynamics of benzene in intense laser fields by tandem mass spectroscopy, J. Chem. Phys. **114**, 5598 (2001).

[20] H. Harada, S. Shimizu, T. Yatsuhashi, S. Sakabe, Y. Izawa, and N. Nakashima, A key factor in parent and fragment ion formation on irradiation with an intense femtosecond laser pulse, Chem. Phys. Lett. **342**, 563 (2001).

[21] L. Robson, K. W. D. Ledingham, A. D. Tasker, P. McKenna, T. McCanny, C. Kosmidis, D. A. Jaroszynski, D. R. Jones, R. C. Issac, and S. Jamieson, Ionisation and fragmentation of polycyclic aromatic hydrocarbons by femtosecond laser pulses at wavelengths resonant with cation transitions, Chem. Phys. Lett. **360**, 382 (2002).

[22] K. Hosaka, A. Yokoyama, K. Yamanouchi, and R. Itakura, Correlation between a photoelectron and a fragment ion in dissociative ionization of ethanol in intense near-infrared laser fields, J. Chem. Phys. **138**, 204301 (2013).

[23] T. Ikuta, K. Hosaka, H. Akagi, A. Yokoyama, K. Yamanouchi, F. Kannari, and R. Itakura, Separation of ionization and subsequent electronic excitation for formation of electronically excited ethanol cation in intense laser fields, J. Phys. B: At. Mol. Opt. Phys. **44**, 191002 (2011).

[24] T. Bohinski, K. Moore Tibbetts, M. Tarazkar, D. Romanov, S. Matsika, and R. J. Levis, Measurement of an electronic resonance in a ground-state, gas-phase acetophenone cation via strong-field mass spectrometry, J. Phys. Chem. Lett. **4**, 1587 (2013).

[25] H. Kono, Y. Sato, M. Kanno, K. Nakai, and T. Kato, Theoretical investigations of the electronic and nuclear dynamics of molecules in intense laser fields: Quantum mechanical wave packet approaches, Bull. Chem. Soc. Jpn. **79**, 196 (2006).

[26] D. Cardoza, B. J. Pearson, and T. Weinacht, Dissociative wave packets and dynamic resonances, J. Chem. Phys. **126**, 084308 (2007).

[27] R. Itakura, K. Yamanouchi, T. Tanabe, T. Okamoto, and F. Kannari, Dissociative ionization of ethanol in chirped intense laser fields, J. Chem. Phys. **119**, 4179 (2003).

[28] H. Yazawa, T. Shioyama, Y. Suda, F. Kannari, R. Itakura, and K. Yamanouchi, Dissociative ionization of ethanol by 400 nm femtosecond laser pulses, J. Chem. Phys. **125**, 184311 (2006).

[29] H. Yazawa, T. Shioyama, Y. Suda, M. Yamanaka, F. Kannari, R. Itakura, and K. Yamanouchi, Controlling the dissociative ionization of ethanol with 800 and 400 nm two-color femtosecond laser pulses, J. Chem. Phys. **127**, 124312 (2007).

[30] H. Yazawa, T. Shioyama, H. Hashimoto, F. Kannari, R. Itakura, and K. Yamanouchi, Non-adiabatic transition in $C_2H_5OH^+$ on a light-dressed potential energy surface by ultrashort pump-and-probe laser pulses, Appl. Phys. B **98**, 275 (2010).

[31] J. Ullrich, R. Moshammer, A. Dorn, R. Dorner, L. P. H. Schmidt, and H. Schmidt-Bocking, Recoil-ion and electron momentum spectroscopy: Reaction-microscopes, Rep. Prog. Phys. **66**, 1463 (2003).

[32] A. M. Rijs, M. H. M. Janssen, E. t. H. Chrysostom, and C. C. Hayden, Femtosecond Coincidence Imaging of Multichannel Multiphoton Dynamics, Phys. Rev. Lett. **92**, 123002 (2004).

[33] A. Matsuda, M. Fushitani, and A. Hishikawa, Electron-ion coincidence momentum imaging of molecular dissociative ionization in intense laser fields: Application to $CS_2$, J. Electron Spectrosc. Relat. Phenom. **169**, 97 (2009).

[34] A. Zhao, P. Sándor, and T. Weinacht, Coincidence velocity map imaging using a single detector, J. Chem. Phys. **147**, 013922 (2017).

[35] D. J. Kane and R. Trebino, Characterization of arbitrary femtosecond pulses using frequency-resolved optical gating, IEEE J. Quantum Electron. **29**, 571 (1993).

[36] T. S. Clement, A. J. Taylor, and D. J. Kane, Single-shot measurement of the amplitude and phase of ultrashort laser pulses in the violet, Opt. Lett. **20**, 70 (1995).

[37] M. Lebech, J. C. Houver, and D. Dowek, Ion–electron velocity vector correlations in dissociative photoionization of simple molecules using electrostatic lenses, Rev. Sci. Instrum. **73**, 1866 (2002).

[38] K. Hosaka, J. Adachi, A. V. Golovin, M. Takahashi, N. Watanabe, and A. Yagishita, Coincidence velocity imaging apparatus for study of angular correlations between photoelectrons and photofragments, Jpn. J. Appl. Phys. **45**, 1841 (2006).

[39] A. S. Alnaser, X. M. Tong, T. Osipov, S. Voss, C. M. Maharjan, B. Shan, Z. Chang, and C. L. Cocke, Laser-peak-intensity calibration using recoil-ion momentum imaging, Phys. Rev. A **70**, 023413 (2004).

[40] S. Katsumata, T. Iwai, and K. Kimura, Photoelectron spectra and sum rule consideration. higher alkyl amines and alcohols, Bull. Chem. Soc. Jpn. **46**, 3391 (1973).

[41] K. M. Refaey and W. A. Chupka, Photoionization of the lower aliphatic alcohols with mass analysis, J. Chem. Phys. **48**, 5205 (1968).

[42] F. Friedman, F. A. Long, and M. Wolfsberg, Study of the mass spectra of the lower aliphatic alcohols, J. Chem. Phys. **27**, 613 (1957).

[43] Y. Niwa, T. Nishimura, and T. Tsuchiya, Ionic dissociation of ethanol studied by photoelectron-photoion coincidence spectroscopy, Int. J. Mass Spectrom. Ion Phys. **42**, 91 (1982).

[44] H.-F. Lu, F. Y. Li, C.-C. Lin, K. Nagaya, I. Chao, and S. H. Lin, The fragmentation of ethanol cation under an electric field: An ab initio/RRKM study, Chem. Phys. Lett. **443**, 178 (2007).

[45] P. R. Bevington and D. K. Robinson, *Data Reduction and Error Analysis for the Physical Sciences*, 2nd ed. (McGraw-Hill, New York, 1992).

[46] W. Zhang, Z. Li, P. Lu, X. Gong, Q. Song, Q. Ji, K. Lin, J. Ma, F. He, H. Zeng, and J. Wu, Photon Energy Deposition in Strong-Field Single Ionization of Multielectron Molecules, Phys. Rev. Lett. **117**, 103002 (2016).

[47] J. Meisner and J. Kästner, Reaction rates and kinetic isotope effects of $H_2 + OH \rightarrow H_2O + H$, J. Chem. Phys. **144**, 174303 (2016).

[48] W. Dietz, H. J. Neusser, U. Boesl, E. W. Schlag, and S. H. Lin, A model for multiphoton ionization mass spectroscopy with application to benzene, Chem. Phys. **66**, 105 (1982).

[49] T. Endo, S. P. Neville, V. Wanie, S. Beaulieu, C. Qu, J. Deschamps, P. Lassonde, B. E. Schmidt, H. Fujise, M. Fushitani *et al.*, Capturing roaming molecular fragments in real time, Science **370**, 1072 (2020).